https://doi.org/10.5194/egusphere-2026-2196
Preprint. Discussion started: 28 July 2026

An automated snow-removal device for radiometers

Jérémie Labelle[a], Pierre-Erik Isabelle[b,d], Benjamin Bouchard[c], Nicolas Breton[a], André Bégin-Drolet[a], Daniel F. Nadeau[b,d]

[a] Department of Mechanical Engineering, Université Laval, 2325 rue de l'Université, Québec, QC, Canada, G1V 0A6

[b] Department of Civil and Water Engineering, Université Laval, 2325 rue de l'Université, Québec, QC, Canada, G1V 0A6

[c] Meteorological Research Division, Environment and Climate Change Canada, 2121 Trans Canada Route, Dorval, QC, Canada, H9P 1J3

[d] Centre for Northern Studies, Pav. Abitibi-Price, Québec, QC, Canada, G1V 0A6

*Corresponding author: daniel.nadeau@gci.ulaval.ca

Abstract

Snowmelt is strongly influenced by shortwave radiation from the Sun and longwave radiation from the Earth and the atmosphere. These energy fluxes are typically measured *in situ* using radiometers equipped with pairs of sensors on the bottom and the top of the housing, which measure upwelling and downwelling radiation respectively. However, measuring under snowy conditions is challenging, as the upper lenses tend to become obstructed by snow. Although heating modules can be integrated into radiometers to prevent frost and dew formation on lenses, they are too energy-intensive for off-grid applications and ineffective against substantial snow build-up. This paper presents a novel snow removal device (SRD) designed to automatically brush snow from radiometers lenses with a per-deployment energy cost equivalent to 17 s of heating. A field campaign over an entire winter season (1 Nov 2024 – 26 Mar 2025) compared a heated and SRD equipped radiometer to a heated-only radiometer, both installed side by side in a snowy forest gap at

https://doi.org/10.5194/egusphere-2026-2196
Preprint. Discussion started: 28 July 2026

Montmorency Forest in Quebec, Canada (47°19′ N, 71°10′ W). Two heating strategies were evaluated during this period: fractional heating (cyclic on/off) and continuous heating. Fractional heating proved to induce noise on the data, while continuously heating systematically left snow around the lenses, resulting in increased longwave measurement (+37.20 MJ m^{-2}) and a decreased shortwave measurement (−1.79 MJ m^{-2}) for the winter period. Heating modules alone are insufficient to ensure high-quality data from radiometers in windless, snowy environments; hence solutions such as the SRD should be prioritized.

1 Introduction

In a context where the cryosphere is undergoing significant changes, such as an increase in winter rain events (Il Jeong & Sushama, 2018), it becomes imperative to develop robust methods for measuring the radiative balance at the Earth's surface. In that sense, net radiation (R_n) is defined as:

$$R_n = \underbrace{(LW_{\downarrow} + SW_{\downarrow})}_{\text{downwelling}} - \underbrace{(LW_{\uparrow} + SW_{\uparrow})}_{\text{upwelling}} \tag{1}$$

where *SW* stands for shortwave radiation (0.3 - 3 µm), *LW* for longwave radiation (4.5 - 42 µm), and where all terms are in W m^{-2}. In (1), arrows pointing down denote downwelling radiation, while arrows pointing up denote upwelling radiation. Accurate measurements of the radiation balance are useful for validating climate model outputs (Huang & Huang, 2023; Irambona *et al.*, 2018), calibrating satellite approaches that seek to estimate surface albedo or surface temperature (Aoki *et al.*, 2011; Liang *et al.*, 2005),

https://doi.org/10.5194/egusphere-2026-2196
Preprint. Discussion started: 28 July 2026

and developing more accurate, physically-based snow models (Gaillard *et al.*, 2025; Jin *et al.*, 1999).

To measure the components of the radiation balance over a snowpack, net radiometers are deployed a few meters above the surface. They consist of two pyranometers and two pyrgeometers, each pair facing upward and downward. The pyranometers respectively measure the downwelling (incident) and upwelling (reflected) shortwave solar radiation, while the pyrgeometers monitor the incident and emitted longwave radiation from the surroundings (ground, sky, clouds, vegetation, etc.). Each sensor converts the incoming radiative energy into an electrical signal through a thermopile. The thermopile relies on a blackened surface that absorbs all incoming radiation within the targeted spectrum (Kipp & Zonen, 2025). The absorbed energy produces a temperature difference relative to a reference plate, typically the metallic base of the instrument, which acts as a heat sink and gradually dissipates energy until thermal equilibrium is reached. The resulting temperature gradient generates a voltage proportional to the net radiative flux. In the shortwave domain, this net flux directly represents the incoming solar radiation, since the sensor itself does not emit radiation in this spectrum. In the longwave domain, however, the sensor emits infrared radiation. Consequently, the thermopile measures the difference between the environment longwave input and the sensor emission. To determine the actual environment contribution, the sensor emission must be taken into account with the following term:

$$Q_{sensor} = \epsilon\sigma T_{sensor}^4 \tag{2}$$

where Q_{sensor} is the longwave emission from the sensor [W m^{-2}], $\sigma = 5.67 \times 10^{-8}$ W m^{-2} K^{-4} is the Stefan–Boltzmann constant, T_{sensor} is the absolute temperature of the sensor [K] and ϵ is equal to 1 since the thermopile sensor is a black body.

https://doi.org/10.5194/egusphere-2026-2196
Preprint. Discussion started: 28 July 2026

Radiometers are integral components of micrometeorological stations to monitor surface energy balance, either during targeted measurement campaigns or as part of more official measurement networks, such as the Baseline Surface Radiation Network (Driemel *et al.*, 2018), ICOS (Heiskanen *et al.*, 2022) or Ameriflux (Novick *et al.*, 2018). In all cases, in cold environments where frost, ice, and snow are present on the measuring lenses, the quality of the measurements can be seriously compromised (Cox *et al.*, 2021; van den Broeke *et al.*, 2004).

For radiometers deployed in cold conditions, ventilators paired with heaters can improve measurement quality (Malek, 2008) by maintaining the temperature of the dome temperature 0.5 - 0.6 °C above the ambient air – sufficient to prevent dew formation and ensure accurate performance (Cox *et al.*, 2021). However, even in the presence of ventilators, it remains a major challenge to distinguish between ice-contaminated data and valid measurements during post-processing (Matsui *et al.*, 2012; van den Broeke *et al.*, 2004). On that topic, Cox *et al.* (2021) conducted a study in which they evaluated 21 heated pyranometers and five heated pyrgeometers in parallel to verify whether ice would be detected by quality control procedures such as QCRAD (Long & Shi, 2008), an automated algorithm which applies a wide set of physically-based limits and consistency checks to identify and correct erroneous radiation measurements. This experiment revealed that ice-contaminated data are particularly difficult to identify because measurement errors caused by ice often fall within the same distribution range as measurements in the presence of clouds. They proposed using cameras paired with daily or hourly inspections as an alternative method of identifying ice on the sensor.

https://doi.org/10.5194/egusphere-2026-2196
Preprint. Discussion started: 28 July 2026

While ice formation on domes is the main challenge in cold and dry regions such as the Arctic, in snowy mid-latitude regions, winds and ventilators cannot prevent snow accumulation, making lens obstruction a major cause of missing/unreliable data (Lapo et al., 2015). This is particularly true in forest environments, where measurements near the ground suffer from the absence of wind, which would otherwise help clear snow from the radiometer – a problem that undermines our understanding of the surface energy balance in these environments. Moreover, remote setups that rely on solar energy often lack the energy resources to sustain ventilator operation (van den Broeke *et al.*, 2004).

To help detect snow-contaminated radiometer data, Lapo *et al.* (2015) developed an algorithm inspired by forest snow interception models, based on local measurements of precipitation, temperature and wind speed. Their algorithm had a snow detection probability of 80% for both of their two sites, with a false alarm rate of 29% and 43%. Although approaches to automate the detection of snow build-up on radiometers exist, such as the method developed by Lapo *et al.* (2015) or the more common, albeit tedious, analysis of hourly trail-camera photos of the instrument – methods to prevent or assess snow accumulation remain scarce. Without solutions to address this issue, the risk of undetected observational errors leading to significant data losses in future studies remains high (Lundquist *et al.*, 2015), although approaches to filling in missing data using machine learning are becoming more effective (Kim *et al.*, 2025). The absence of standardized heating algorithms for radiometers in snowy conditions also leads to inconsistent mitigation practices (ventilation, manual snow removal, data replacement), raising major concerns for data reliability (Kim *et al.*, 2025).

https://doi.org/10.5194/egusphere-2026-2196
Preprint. Discussion started: 28 July 2026

To the best of our knowledge, the only radiometer setup equipped with an automated snow-removal system is the one used by Météo-France at Col de Porte, which was installed in the 1980s - 1990s (Morin *et al.*, 2012). It consists of two 1.5 m arms arranged in a V shape on a 3 m steel mast with a cross-section of 15 cm × 15 cm, carrying the radiometers. The arms are mounted on a plate that can move vertically with a rack-and-pinion mechanism to maintain a fixed distance from the snow surface. The arms can also rotate horizontally to position the sensors within a cleaning enclosure. This rotation is driven by a 220 V motor with a chain and sprocket transmission. When moving within the enclosure, flexible brushes remove the snow, and hot air eliminates any remaining snow or water for approximately 2.5 min. Cleaning cycles are triggered automatically each hour. This system has proven to be robust, requiring only one motor replacement after several decades of operation (Y. Lejeune, personal communication). However, replicating such a mechanism on existing installations would be difficult due to its large size, mechanical complexity, and high-power requirements.

Considering this, there is a need to develop a compact, low-power device capable of removing snow from radiometers that can be installed on existing setups. The objectives of this study are therefore: 1) to present a new automated snow-removal device for radiometers, 2) to monitor its energy consumption, 3) to explore the effect of the heating strategy on data quality, 4) to evaluate the impact of the automated snow-removal device on measurements of the radiation balance.

https://doi.org/10.5194/egusphere-2026-2196
Preprint. Discussion started: 28 July 2026

2 Materials and methods

2.1 Study site and meteorological conditions

The study site is located at the Montmorency Forest (MF), a long-term experimental site located approximately 80 km north of Quebec City (47°19′ N, 71°10′ W) in Canada (Fig. 1a). The MF spans approximately 412 km² and is a balsam fir-dominated ecosystem representative of the humid boreal forest (Isabelle *et al.*, 2020), with elevations ranging from 600 to 1000 m above sea level (ASL). The region experiences a continental subarctic climate, with a mean annual total precipitation of 1502 mm, of which 602 mm (40%) falls as solid precipitation, based on climate data computed for the period 1991 - 2020 (Environment and Climate Change Canada, Montmorency Forest, station ID 7042388).

The MF hosts a dedicated snow research site (the NEIGE site; 1.1 ha, 665 m ASL) that has previously been used for research on solid precipitation undercatch (Pierre *et al.*, 2019) and on contrasting methods to measure snow water equivalent (Beaudoin-Galaise & Jutras, 2022). A small forest gap with a radius of 4 m some 100 m northeast of the NEIGE site was selected as our main study site (hence referred to as the *NEIGE gap*), where near-surface winds are very weak in winter and thus 'favours' snow building up on the radiometers. Radiation measurements in isolated forest gaps are not rare in forest meteorology and snow hydrology applications (Isabelle *et al.*, 2018; Malle *et al.*, 2019; Musselman *et al.*, 2015). However, the choice of this site comes with challenges related to the spatial variability of incident radiation within the gap.

https://doi.org/10.5194/egusphere-2026-2196
Preprint. Discussion started: 28 July 2026

2.2 Experimental site and setup

The experimental setup consisted of two net radiometers (CNR4, Kipp & Zonen, the Netherlands) that were mounted side by side in the NEIGE gap (see Fig. 1c). The setup was installed on 1 November 2024 and the period of analysis spanned until the last appearance of snow on the radiometers (26 March 2025), with a sampling frequency of 1 min. The radiometers were placed 50 cm apart to make sure the snow accumulation on one would not affect the other. Both instruments were mounted at a height of 2.7 m above ground and equipped with a heating module consisting of a ventilator and a heater (CNF4, Kipp & Zonen, the Netherlands). According to the supplier, each heating module draws 15 W when activated.

One of the two radiometers, referred to as the *snow-cleared radiometer*, was equipped with the snow-removal device (SRD), shown in Fig. 1c-d. The second radiometer was not equipped with an SRD and thus served as the *control radiometer*. The SRD is a custom-built telescopic brush that allows to automatically clears snow from the top of a radiometer. The design of this device is explained in greater details in section 2.5.

https://doi.org/10.5194/egusphere-2026-2196
Preprint. Discussion started: 28 July 2026

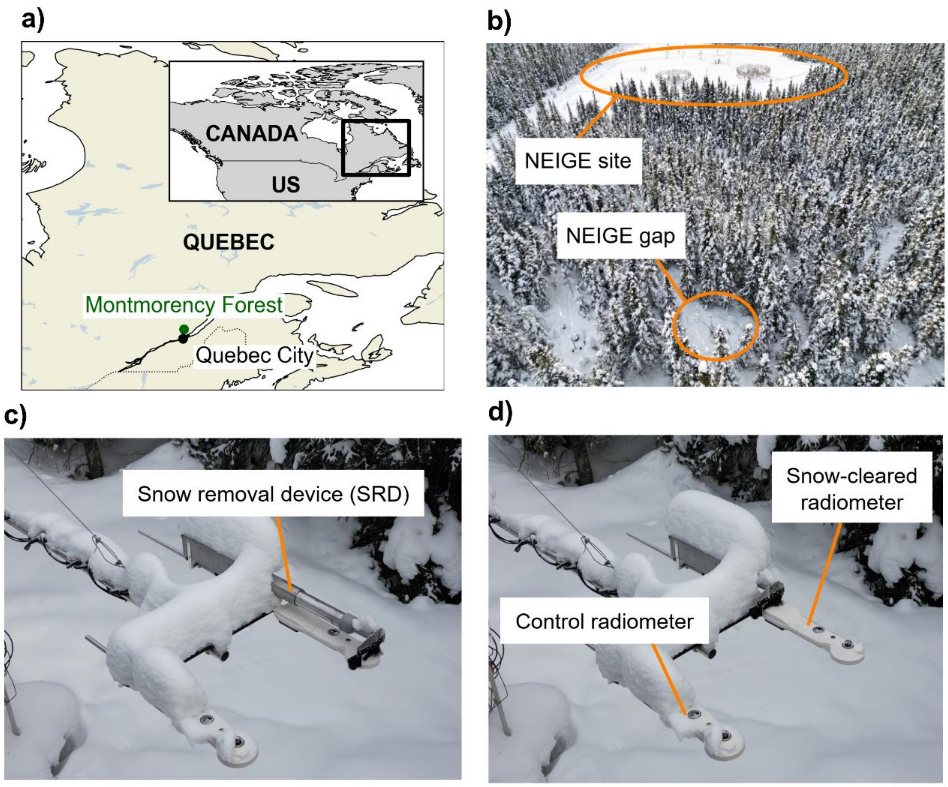

Fig. 1. Location and photos of the experimental setup in the province of Quebec, Canada; a) location of the experimental site; b) aerial view of the NEIGE gap, located about 100 m from the NEIGE site (photo taken on 12 December 2024); c) closeup of the snow-removal device (SRD) in its extended configuration; d) SRD in its retracted configuration, with the two radiometers identified. Photos in c) and d) were taken on 23 January 2025.

Although the SRD was originally meant to run on solar panels and batteries during winter, the test campaign used grid power instead. A backup battery was added so the system could keep running in case of a power outage. Using the electrical grid made it possible to monitor the setup more easily through real-time IoT tools and ensured the experiment would not shut down due to a lack of energy.

Both radiometer data were acquired by a CR6 datalogger (Campbell Scientific, USA) every 5 s and averaged every minute. Photos of the setup were collected hourly with an AXIS

https://doi.org/10.5194/egusphere-2026-2196
Preprint. Discussion started: 28 July 2026

PTZ camera (Axis Communications, Sweden). Photos were also taken at three specific moments during the deployment of the SRD: at the start, at maximum extension (extended configuration), and upon return to the starting position. Timeouts were programmed to ensure that a photo would still be taken even if the SRD did not work as expected (for example, if it did not reach the farthest point or did not return to the retracted position).

2.3 Heating strategies

While it is clear that heating modules in radiometers are necessary and should be turned on when possible, their large power consumption implies the need to manage their usage in power-limited setups. However, there does not appear to be a consensus on which strategy to implement to turn on the heating module (Campbell Scientific, personal communication). For setups with limited energy availability, heaters can be programmed to start when humidity is high or at sunset and sunrise (Campbell Scientific, 2025), or can even be turned off all throughout winter (van den Broeke et al., 2004). To represent this variability in heating schemes, two strategies were tested: for the first part of the winter period, fractional heating was applied, whereas continuous heating was applied for the second part.

Fractional heating (FH)

In the first data segment, ranging from 1 November 2024 to 12 December 2024 (40 days), an intermittent heating strategy was used, *i.e.*, a 5-min heating cycle followed by a 25-min pause, which will be referred to in this work as *fractional heating* or FH. Heating modules were asynchronous by a 15-min phase to prevent excessive voltage drop on the power system. This type of heating is usually used for remote sites with a limited supply of energy.

https://doi.org/10.5194/egusphere-2026-2196
Preprint. Discussion started: 28 July 2026

By 12 December 2024, enough data had been gathered to draw conclusions from this heating strategy.

Continuous heating (CH)

In the second data segment, ranging from 13 December 2024 to 26 March 2025, heating was activated all the time, a period referred to as *continuous heating* or CH. This method represents the ideal situation where there would be an unlimited power source. This period lasted until the last appearance of snow on the device.

2.4 Timeline and dates with modifications or maintenance on the setup

To accommodate for failures of the SRD (due to freezing rain in December), the maximum current limit had to be raised from 1 A to 2 A on 20 December 2024, something discussed in greater details in section 4.1. Snow was cleared from both devices during each site visit (listed in Table 1), thereby resetting the snow accumulation on the full setup.

Table 1. Important dates and changes applied to the setup during the winter campaign.

Date	**Event description**	**Manual snow removal**
2024-11-26	SRD blocked for 1 day because of freezing rain	-
2024-12-12	SRD blocked for 8 days because of freezing rain	-
2024-12-20	Current limit on the SRD increased from 1 A to 2 A	Yes
2024-12-26	SRD blocked for 1 day because of freezing rain	-
2025-01-12	Maintenance visit	Yes
2025-01-23	Maintenance visit	Yes
2025-02-20	Maintenance visit	Yes

2.5 SRD design

The SRD was designed as a complementary tool to heating. As such, it focused on the limitations of the heating modules. Frost and dew on the domes are better mitigated by the

https://doi.org/10.5194/egusphere-2026-2196
Preprint. Discussion started: 28 July 2026

heating system, while the SRD is better suited for removing snow accumulation. Requirements for the SRD device were low power (< 1 A for around 1 min), high mechanical reliability, and limited obstruction of the radiometer field of view.

The system features a telescopic brush that was designed to push snow off the top of the radiometer. With a reach of 370 mm, the SRD was designed to extend through the full length of the radiometer (in our case a CNR4) and its integrated heater. Weighing around 7 kg, it was designed to be mounted on the radiometer support rod using U-bolts. A broom-style tip was selected instead of a scraper, as any snow that froze onto the radiometer would be more efficiently removed by a heating module. The entire system is driven by a 12 V, 20 W motor (ANDYMARK NeveRest Orbital 20), with limit switches installed at the beginning and end of the brush motion to confirm successful motion and inform on the position of the brush. To monitor the displacement of the brush through time, an encoder was installed to record the angular position of the motor.

During a deployment, the mechanism was designed to follow a precise sequence: it initially moved backwards until the initial limit switch was toggled (this is to make sure it always started its motion at the zero position in case the previous deployment did not work properly), the brush then moved forward until reaching the forward limit switch, to then return back to the initial switch, and finally moved slightly forward to clear the limit switch contact.

From the radiometer lens perspective, the SRD subtends a solid angle of approximately 7° × 7°, corresponding to approximately 0.23% of the 180° field of view of the upper pyranometer and pyrgeometer.

https://doi.org/10.5194/egusphere-2026-2196
Preprint. Discussion started: 28 July 2026

In the absence of a reliable algorithm to automatically detect snow, deployments were scheduled at fixed intervals: 00:10, 04:10, 08:10, 10:10, 11:10, 12:10, 13:10, 14:10, 15:10, 17:10, and 20:10 (local time). The reason why they were 10 min late to the hour was to avoid powering heaters at the same time as the SRD when heating fractionally, something that was initially tough to be a potential issue but later revealed to be insignificant.

2.6 *SRD deployment performance and failure modes*

During this experimental period, four deployment types occurred. The first represented proper operation of the device, while the other three represented mechanical malfunctions.

1) *Normal deployment*: the SRD extended and returned to its retracted position in less than 40 s, consuming less than 0.9 A.
2) *Failed deployment*: the SRD could not be deployed or returned to its retracted position.
3) *Slow deployment*: the SRD could be deployed and returned to its retracted position, but did so in more than 40 s.
4) *High-current deployment*: the SRD could be deployed and returned to its retracted position but drew more than 0.9 A from the 12 V power supply.

The reliability of the SRD was assessed by sorting every deployment into one of these four categories.

2.7 *Sign convention for control vs. snow-cleared radiometers*

To compare the measurements from the two radiometers, the difference in measured radiation (ΔR_n) is determined by subtracting the data from the snow-cleared radiometer from that of the control radiometer:

https://doi.org/10.5194/egusphere-2026-2196
Preprint. Discussion started: 28 July 2026

$$\Delta R_n = R_{n,\,\text{control}} - R_{n,\,\text{snow-cleared}} \tag{3}$$

Similarly, the net radiation difference can be written as the signed sum of the differences in all radiative components, with incoming fluxes contributing positively and outgoing fluxes contributing negatively:

$$\Delta R_n = +\,\Delta LW_{\downarrow} + \Delta SW_{\downarrow} - \Delta LW_{\uparrow} - \Delta SW_{\uparrow} \tag{4}$$

This means a positive ΔR_n occurs when the control radiometer reports a larger measurement than the snow-cleared radiometer, whereas a negative ΔR_n indicates that the control radiometer reports a smaller measurement than the snow-removed radiometer.

2.8 Labelling days when the control radiometer was contaminated by snow

Since the snow-cleared radiometer remained mostly free of snow throughout the winter, the identification of snow-covered days was based on the control radiometer. The presence of snow on the control radiometer was determined from hourly photographs. Days were classified into one of the two categories:

- *Snow-covered days* (70 occurrences) if any amount of snow was present on or near the control radiometer top lenses (Fig. 2a) – even when only a small portion of a single lens was affected (Fig. 2b).
- *Snow-free days* (75 occurrences) if the control radiometer was clear of any snow (Fig. 2c-d).

The contour of the photos on Fig. 2 is related to the color code in the subsequent figures: orange is used to mark snowy days, and blue to mark snow-free days.

https://doi.org/10.5194/egusphere-2026-2196
Preprint. Discussion started: 28 July 2026

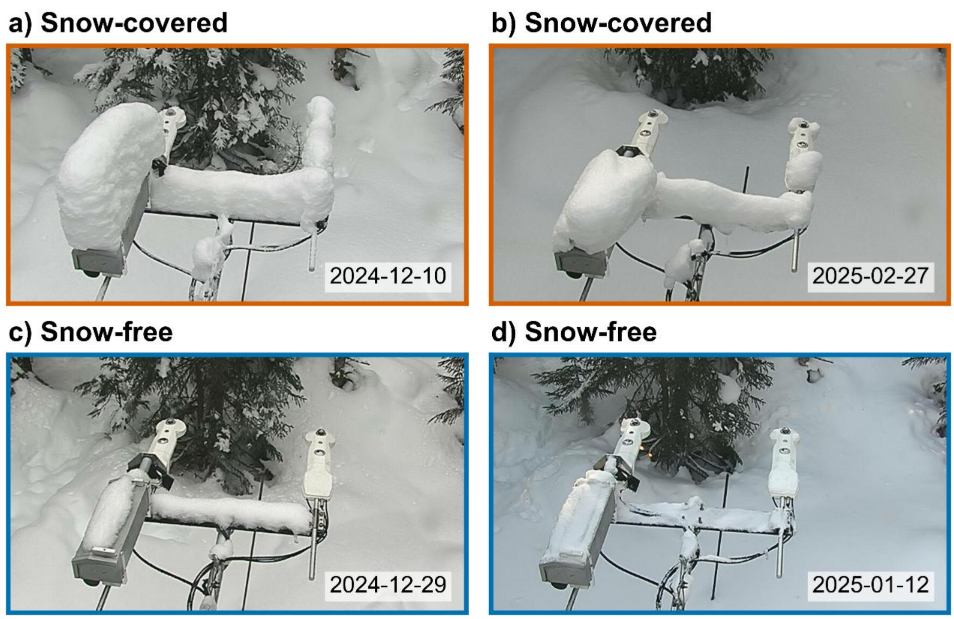

Fig. 2. Examples of the classification for the presence snow on the setup. a) Major snow accumulation on the control radiometer. b) A small presence of snow near the lenses of the control radiometer. c) and d) Control radiometer is snow-free.

Something to be noted in Fig. 2a is the height of the snow accumulation on top of the SRD housing, a limitation of the current design (see section 4.1).

3 Results

3.1 Weather conditions during the winter field campaign

During the study period, the coldest temperature recorded 2 m above ground at the NEIGE site was −36 °C (12 February 2025) and the warmest temperature recorded was 13.9 °C (20 March 2025), with an average of −9 °C. The first snowfall was recorded on 27 November 2024, and the last one on 24 March 2025. The maximum snowpack height was measured at 115 cm in early March from the station at NEIGE site. Total precipitation

https://doi.org/10.5194/egusphere-2026-2196
Preprint. Discussion started: 28 July 2026

measured at the NEIGE site during the study period using a DFAR (Double Fence Automated Reference) precipitation gauge was 528 mm. During the study period, four rain-on-snow events were recorded, contributing a total of 76 mm (14.3 % of the total precipitation).

3.2 SRD reliability and energy consumption

Table 2 shows the 1472 SRD deployments that occurred during the study period and were classified according to the method described in section 2.6.

Table 2: Classification of SRD deployments during the winter of 2024-25.

Deployment type		Number of occurrences	%
Normal		1184	81
Failed		58	4
Slow		107	7
High current		123	8
	Total	1472	-

Fig. 3 shows the current consumption, distance travelled, and energy consumption of the SRD. In terms of energy consumption, the SRD required an average of 248 J per deployment (across all deployment types), equivalent to operating the heater for 17 s. With 11 deployments per day, the total energy used by the SRD for the full winter was 370000 J, which is equivalent to 7 h of heating. For days with frequent failed deployments (primarily between 12 to 20 December 2024), the radiometer data were discarded. This exclusion applies to all subsequent analyses presented in this paper.

https://doi.org/10.5194/egusphere-2026-2196
Preprint. Discussion started: 28 July 2026

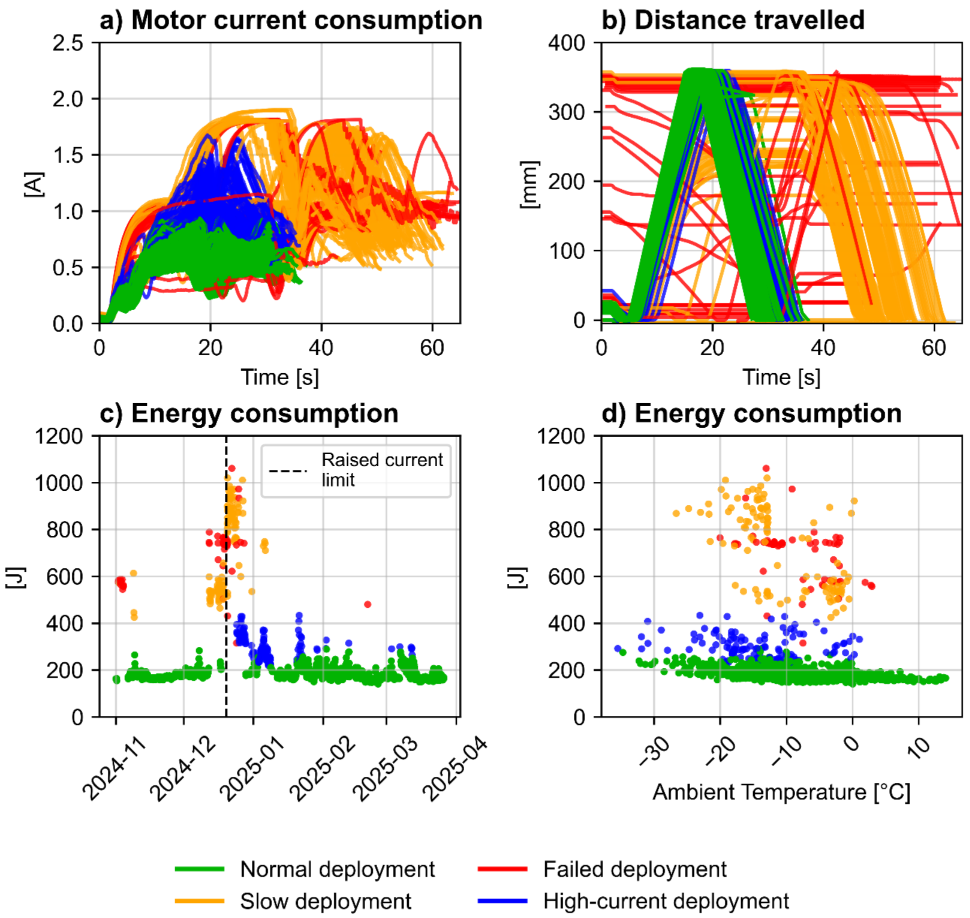

Fig. 3. Logs from every deployment of the SRD. a) Total current measured by the SRD. b) Distance travelled by the brush of the SRD. c) Total energy consumed for every deployment. On 20 December 2024, the current limit was increased from 1 A to 2 A, marked here by a dashed vertical line. d) Energy consumed for every deployment versus air temperature.

3.3 Thermal artifacts from fractional heating

The frequency of measurements used in this study (every minute) allowed to discover undesirable effects from fractional heating. Since radiometers are devices that operate based on thermal stability between the top and bottom of the thermopile, turning the heating

https://doi.org/10.5194/egusphere-2026-2196
Preprint. Discussion started: 28 July 2026

319 on and off at regular intervals induce a transient state that degrades the quality of the
320 measurements (Fig. 4).

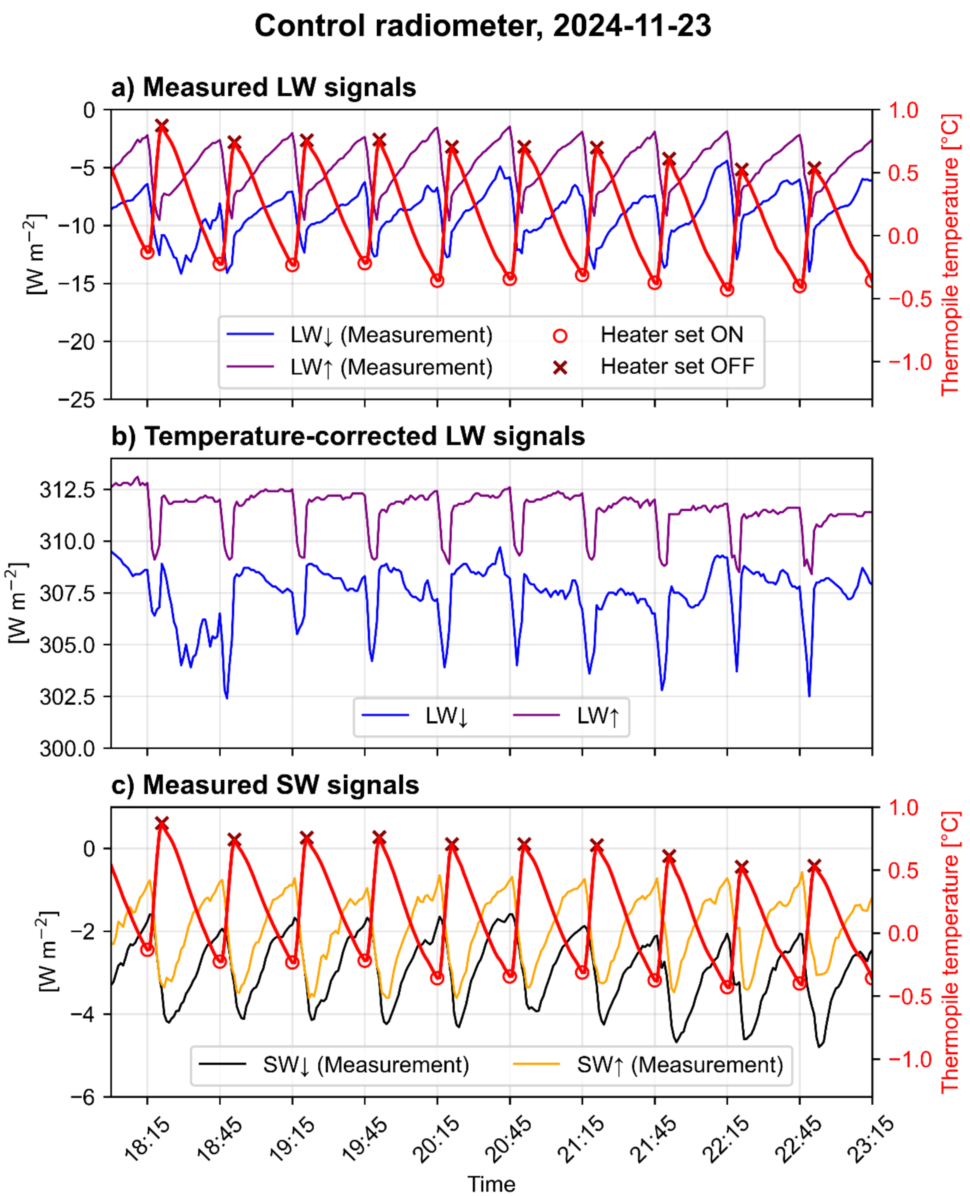

321
322 *Fig. 4. Example of fractional heating and the effects associated on the measured signals;*
323 *(a) comparison of the raw thermopile longwave radiation measurements with the internal*
324 *temperature of the radiometer; (b) longwave radiation measurements with the temperature*

https://doi.org/10.5194/egusphere-2026-2196
Preprint. Discussion started: 28 July 2026

correction applied onto the raw signal; (c) comparison the shortwave radiation measurements with the internal temperature of the radiometer.

Every temperature spike (red) is associated with the ventilation/heater being turned on and subsequently off, slowly going back to air temperature. All thermopile signals present an inverse linear relationship with the temperature. Fig. 4b presents temperature corrected $LW_{\uparrow}$ and $LW_{\downarrow}$ signals (eq. 2). Even with temperature corrected algorithms, both $LW_{\uparrow}$ and $LW_{\downarrow}$ signals experience a significant downwards spike when heating is activated.

As fractional heating introduced significant measurement noise, all subsequent analyses identify and label data from this period separately from data collected under continuous heating.

3.4 Agreement plots for the radiometers

For radiometers installed in the NEIGE gap, direct sunlight (SW) interacts strongly with the surrounding trees. At a given time of day, one radiometer may be shaded while the other receives direct sunlight. This leads to some discrepancy between the two sensors, making comparison of high-frequency data difficult. This problem is minimized when using daily sums, which provides a measurement easier to interpret. As such, Fig. 5 shows the agreement between daily sums of incoming shortwave radiation under snow-free (blue) and snow-covered conditions, both during fractional (brown, 1 November – 11 December 2024) and continuous (orange, 12 December 2024 – 26 March 2025) heating.

https://doi.org/10.5194/egusphere-2026-2196
Preprint. Discussion started: 28 July 2026

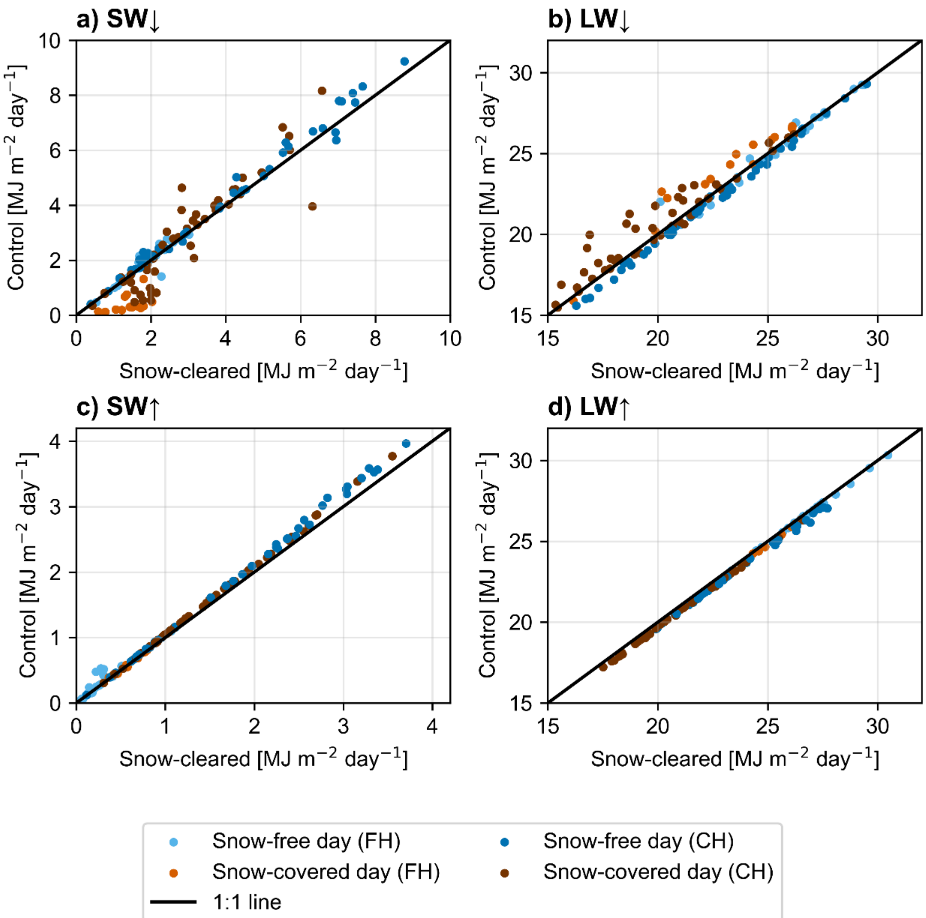

Fig. 5. Scatter plot comparing radiation daily sums from the control radiometer to the snow-cleared radiometer, for a) downwelling shortwave radiation (solar); b) downwelling longwave radiation; c) upwelling shortwave radiation; and d) upwelling longwave radiation. Orange/brown dots represent days the control radiometer was snow-covered whereas blue/cyan dots represent days when the control radiometer was snow-free.

From examining the downwelling shortwave radiation comparison (Fig. 5a), the presence of snow on the control radiometer (orange and brown dots) leads to one of two distinctive patterns: radiation measurements that are consistently lower than those of the snow-cleared sensor when the daily sum is small ($SW_{\downarrow}$ < 2.5 MJ m^{-2}), and radiation measurements that may be higher or lower than those of the snow-cleared radiometer when the daily sums are

https://doi.org/10.5194/egusphere-2026-2196
Preprint. Discussion started: 28 July 2026

large ($SW_{\downarrow}$ > 2.5 MJ m^{-2}). In the first pattern, small daily sums are linked to cloudy conditions, and thus to potential snowfall events. Under these circumstances, the control radiometer likely accumulated snow on its lens with insufficient heating to melt it. Because fresh snow is highly reflective in the shortwave spectrum, limited incoming radiation was able to reach the lens, resulting in a strongly reduced signal. Days with fractional heating led to larger reductions of the signal (orange dots), as the available energy from the heating module was insufficient to melt the accumulated snow. For the second pattern, larger daily sums were typically associated with sunny days. In that scenario, Fig. 5a shows that the presence of snow on the radiometers can either amplify or attenuate the radiation measurement (brown dots). However, noticeable are some snow-covered days with radiometers giving comparable measurements, suggesting amplification and attenuation effects that cancel each other. More information on phenomena that can lead to signal amplification is presented and discussed in section 3.7.

Fig. 5b shows downwelling longwave radiation ($LW_{\downarrow}$), which was almost systematically higher on the control radiometer than on the snow-cleared radiometer when snow was present on the control device (orange dots), regardless of the heating strategy. This can be explained by the fact that snow acts as an additional source of longwave radiation, being warmer than the effective temperature associated with incoming longwave radiation from the atmosphere and surrounding canopy. Conversely, both radiometers show strong agreement (blue dots) when snow-free, with what appears to be a small negative systematic bias between devices.

The upwelling shortwave and longwave radiation signals ($SW_{\uparrow}$ and $LW_{\uparrow}$, Fig. 5c–d) were highly consistent between the two devices. A systematic negative bias for both longwave

https://doi.org/10.5194/egusphere-2026-2196
Preprint. Discussion started: 28 July 2026

measurements is also observed. Inversely, a positive bias for the control radiometer is seen for high upwelling shortwave radiation, which might be caused by heterogeneities on the ground below the devices.

3.5 Differences between radiometers with and without snow

Fig. 6 shows the differences in daily sums of radiation between the two radiometers for each radiation component: $\Delta SW_{\downarrow}$, $\Delta LW_{\downarrow}$, $\Delta SW_{\uparrow}$, $\Delta LW_{\uparrow}$, and finally for net radiation ΔR_n. Note that a positive value indicates that the measurement taken by the control radiometer is greater than that taken by the snow-cleared radiometer. The distribution pattern shows how radiometer measurements diverge with and without snow. For each plot, the blue distribution represents the difference when both radiometers were under snow-free conditions, serving as a baseline or "expected" difference between the instruments. In contrast, the orange distributions represent the difference for days when the control radiometer was snow-covered, thereby highlighting the differences induced by the presence of snow. This analysis enables the snow-induced biases to be separated from the baseline (systematic) differences, providing a clearer comparison between the two radiometers and preventing distinct sources of error from being confused. It is important to note that the results presented in Fig. 6 are based solely on data collected between 1 January and 26 March 2025, in order to exclude data from the fractional heating period and periods of equipment malfunction in mid-December 2024. Summer data for these distributions are also shown in Fig. A1. The summer distributions closely resemble those observed in winter in the absence of snow, suggesting that snow-free biases presented here are related to the devices and their position, and not to effects related to the presence of snow on the ground or in the forest canopy.

https://doi.org/10.5194/egusphere-2026-2196
Preprint. Discussion started: 28 July 2026

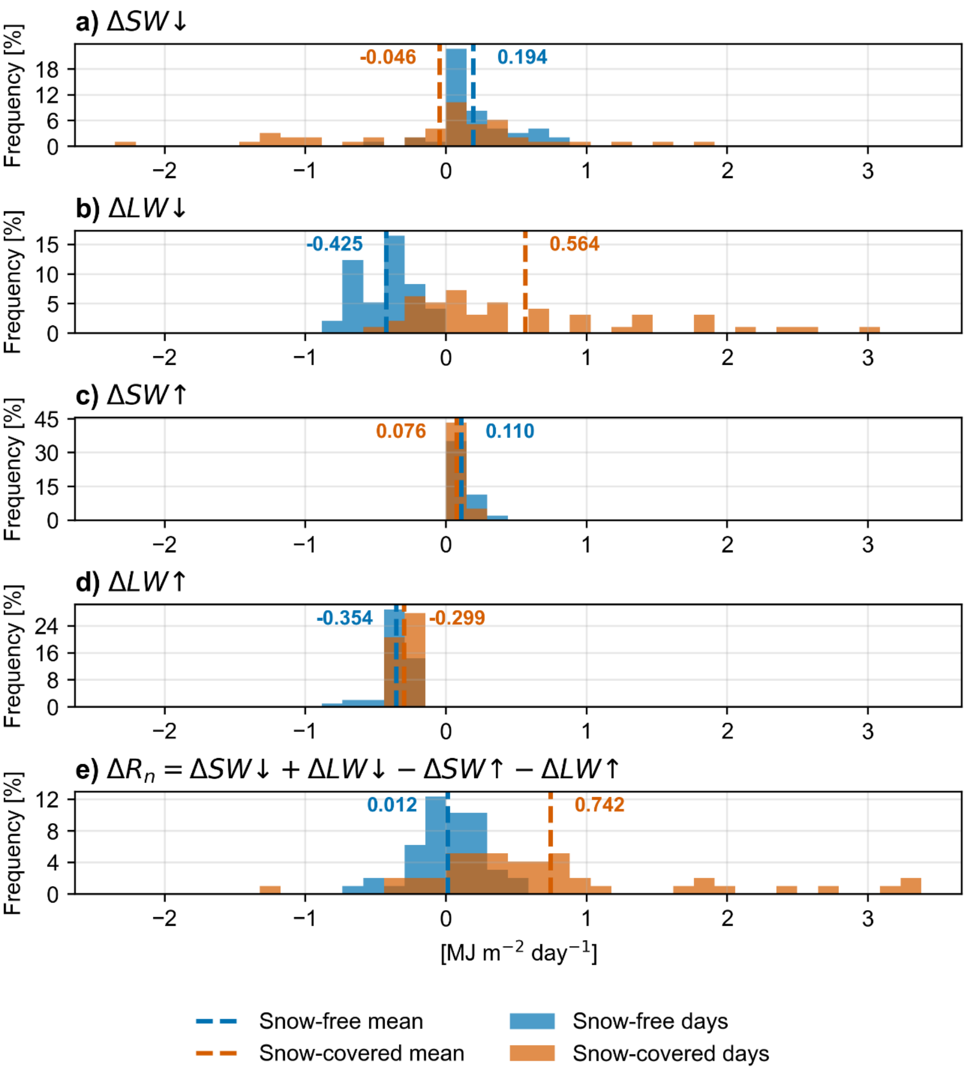

Fig. 6. Daily energy differences (control minus snow-cleared radiometer data) between the two radiometers represented as histograms and classified according to snow-free days (blue) and snow-covered days (orange) on the control radiometer. Dotted lines show the mean value (also printed out) of each group. Data are plotted from 1 January to 26 March 2025.

For $\Delta SW_{\downarrow}$ (Fig. 5a), the mean difference is 0.194 MJ m^{-2} day^{-1} under snow-free conditions, and −0.046 MJ m^{-2} day^{-1} when snow-covered. As the difference shifts from positive to

https://doi.org/10.5194/egusphere-2026-2196
Preprint. Discussion started: 28 July 2026

negative, the net effect of snow on the control radiometer is an average decrease in incoming shortwave energy ($SW_{\downarrow}$) of 0.240 MJ m^{-2} day^{-1}.

For $\Delta LW_{\downarrow}$ (Fig. 5b), the mean difference under snow-free conditions is −0.425 MJ m^{-2} day^{-1}, indicating a systematic offset likely related to differences in instrument characteristics, but also in the sky view fractions. This difference remains consistent throughout the summer period, as shown in Fig. A1. This suggests that the control radiometer tends to measure less $LW_{\downarrow}$ than the SRD-equipped radiometer. However, under snow-covered conditions, the bias shifts from −0.425 MJ m^{-2} day^{-1} to +0.564 MJ m^{-2} day^{-1}. This reversal reflects a substantial increase in incoming longwave radiation when the control radiometer is snow-covered. On average, the net increase caused by snow in the longwave is +1.014 MJ m^{-2} day^{-1}, that is +11.73 W m^{-2} over a 24-h period.

Upwelling components ($\Delta LW_{\uparrow}$ and $\Delta SW_{\uparrow}$) are shown in Fig. 5c-d. The variability between both devices is much smaller than their downwelling counterparts, even under snow-covered conditions, indicating that both radiometers remain in close agreement despite the snow on their upper lenses. However, the daily difference in longwave upwelling radiation ($\Delta LW_{\uparrow}$) exhibits a mean difference of −0.354 MJ m^{-2} day^{-1} regardless of snow accumulation or not on the control radiometer. Interestingly, the downwelling longwave component ($\Delta LW_{\downarrow}$) exhibits a similar bias without the presence of snow (−0.425 MJ m^{-2} day^{-1}).

Fig. 6e is the addition of all these effects, expressed as R_n. This figure illustrates the summation of snow-induced and systematic differences in the net radiation measurements. The snow-free biases (blue distributions) from each component almost cancel each other out, resulting in a daily net radiation energy difference of just 0.012 MJ m^{-2} day^{-1}. On the

https://doi.org/10.5194/egusphere-2026-2196
Preprint. Discussion started: 28 July 2026

other hand, the net radiation measurement is amplified by an average of 0.742 MJ m^{-2} day^{-1} when the control radiometer is snow-covered, which is equivalent to an increase of 8.58 W m^{-2} over a 24-h period.

3.6 Cumulative net radiation

Fig. 7 presents the cumulative energy calculated from measurements taken by the two radiometers between 1 January and the end of the measurement campaign on 26 March 2025, avoiding the fractional heating period and the SRD failures observed in December 2024. Net radiation (Fig. 6a), net longwave (Fig. 6b) and net shortwave (Fig. 6c) are displayed to compare the contribution of each component. Snow-free days are distinguished from snow-covered days with respectively white and grey backgrounds.

https://doi.org/10.5194/egusphere-2026-2196
Preprint. Discussion started: 28 July 2026

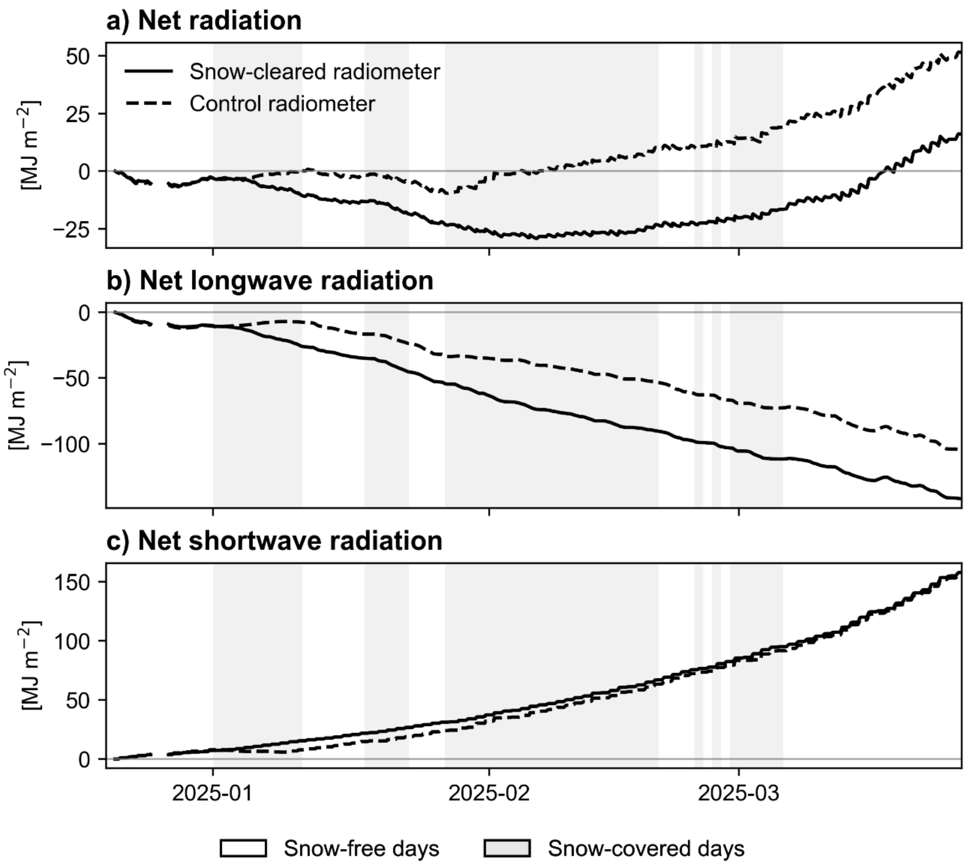

Fig. 7: Cumulative radiative energy from the two radiometers from 1 January to 26 March 2025: a) net radiation; b) net longwave radiation; c) net shortwave radiation. The solid lines represent the snow-cleared radiometer, while the dashed lines represent the control radiometer. The white bands represent snow-free days, while the gray bands represent days with snow.

The figure clearly highlights the errors induced by a snow-covered radiometer. Indeed, longwave radiation is systematically overestimated when snow accumulates on the sensor. This effect is evident in Fig. 7b, where a snow event (grey) corresponds to an increasing divergence between the two curves. For shortwave radiation, the divergence between the two sensors remains limited. The previously mentioned increases and decreases tend to

https://doi.org/10.5194/egusphere-2026-2196
Preprint. Discussion started: 28 July 2026

compensate each other, yielding a signal that is overall comparable to that of the snow-cleared radiometer.

These concurring errors result in the net radiation of the control radiometer reaching the zero line 43 days earlier than that of the snow-cleared device (Fig. 7a). In fact, the difference in net radiation between the devices at the end of the period is 35.41 MJ m^{-2}, the difference in net longwave is 37.20 MJ m^{-2}, and finally the net shortwave difference is $-$1.79 MJ m^{-2}. It should be noted that these differences are conservative and that the discrepancy between the two devices would have been even greater if no manual snow removal had been carried out on the devices on 12 January, 23 January, and 20 February 2025 (see Table 1).

3.7 Shortwave increase and light funnel effect

Fig. 8 presents typical shortwave radiation readings taken at our site on two clear-sky days. Fig. 8a-b are from a day affected by a 'light funnel effect' on the control radiometer, while Fig. 8c-d are from a day when there was no snow on the devices. The light funnel effect occurs when snow above the lens melts, leaving a cavity that channels additional light toward the sensor, artificially enhancing the measured downwelling shortwave. From the moment continuous heating was applied, this behavior was observed on every visit. It was also occasionally observed in the camera images, but the camera angle sometimes made identification difficult.

https://doi.org/10.5194/egusphere-2026-2196
Preprint. Discussion started: 28 July 2026

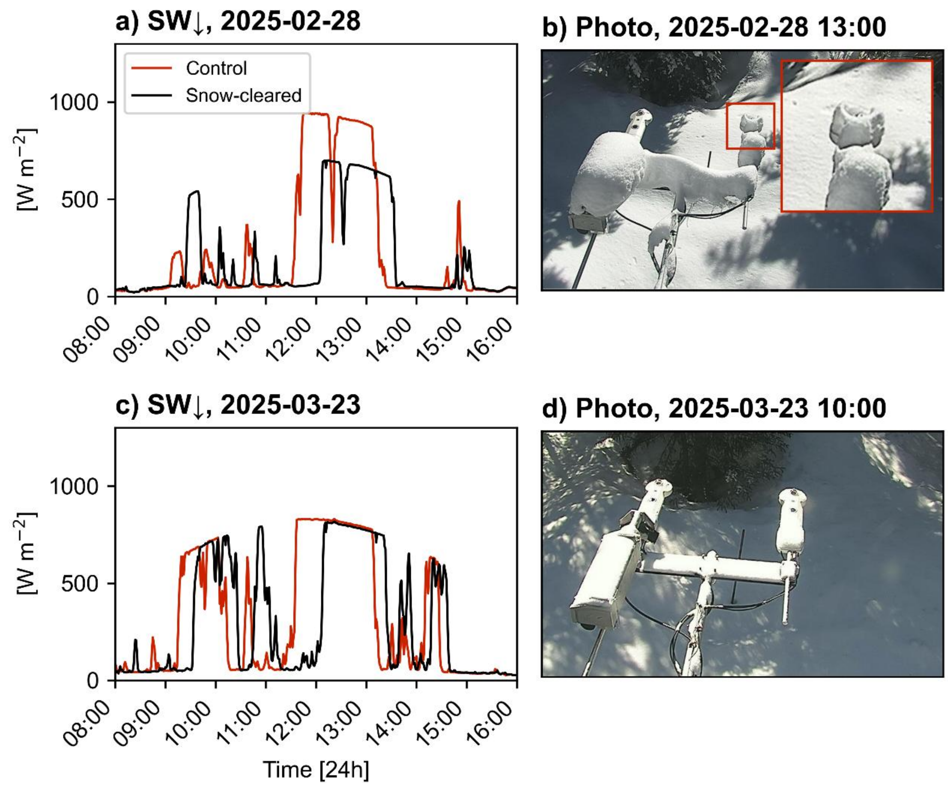

Fig. 8. (a) Overestimated shortwave radiation measurements due to the light funnel effect; (b) photo taken while the control radiometer was under the light funnel effect; (c) normal signal under clear-sky conditions; (d) photo taken while both radiometers were free of any snow and under clear-sky conditions.

4 Discussion

4.1 SRD efficiency, reliability, and design considerations

With 11 deployments per day, the SRD consumed 0.3% of the energy required for continuous heating. Most of this energy was spent overcoming friction forces. Current heating modules are energy-intensive and ineffective at removing snow from radiometers. The data from this campaign showed that pairing the SRD with heating is a promising

https://doi.org/10.5194/egusphere-2026-2196
Preprint. Discussion started: 28 July 2026

approach to improve radiometer measurements in cold climates. The SRD removes the bulk of the accumulated snow, while adding only a marginal energy cost.

In terms of reliability, the main issues revolved around freezing rain. In particular, the freezing rain event on 12 December 2024 (duration: 17 h, total rainfall: 15.5 mm, mean air temperature: –1.0°C) followed by a significant temperature drop (–13°C) caused some failures (Fig. 3c). On-site observations suggest that a thin layer of water froze around the SRD telescopic cylinders during their deployment. This ice increased the cylinder's effective diameter and reduced the clearance between the moving parts, resulting in a mechanical blockage. Supplying additional current to the motor driving the mechanism enabled the SRD to complete its cycle, with each operation progressively removing part of the ice layer. This can be observed from 20 December 2024 (when the current limit was increased) in Fig. 3c: with more current available, the average energy consumption increased for a few days, meaning that although it struggled, the mechanism still worked (yellow dots). For the rest of the winter, many deployments drew more than 1 A, yet still functioned properly, meaning the mechanism required more power to work in harsher conditions.

Fig. 3d shows that there is little to no correlation between temperature and energy consumption for the SRD, since most of the abnormalities are well dispersed across all temperatures. Fig. 3c also shows that the system performed well at temperatures below ¯20°C, which was an important requirement for such a device.

https://doi.org/10.5194/egusphere-2026-2196
Preprint. Discussion started: 28 July 2026

4.2 Continuous heating limitations

Fig. 9 presents snow pockets around the pyrgeometer created by the heating module. This phenomenon could only be documented during two site visits, as the monitoring camera was positioned behind the radiometers and could not capture it properly.

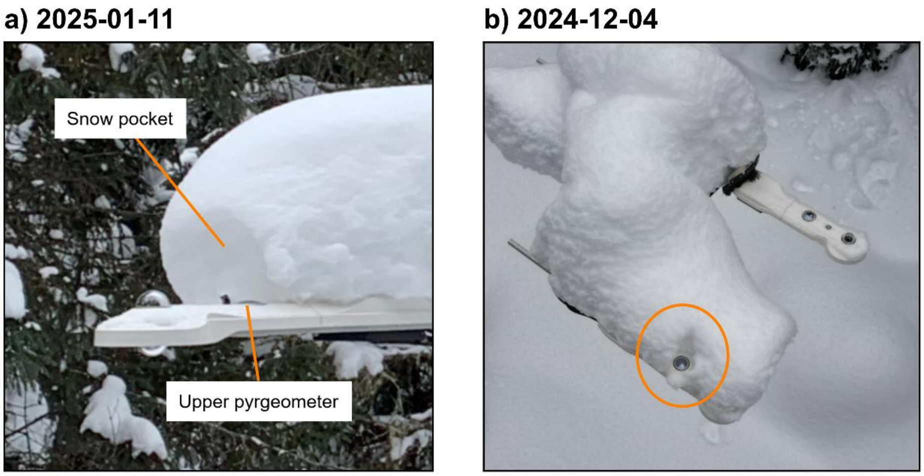

Fig. 9. Anomalies caused by heating: (a) a snow pocket above the pyrgeometer, while the pyranometer remains snow-free (photo taken on 11 January 2025, with continuous heating); (b) a snow pocket above the pyrgeometer, while the pyranometer is fully covered in snow (photo taken on 4 December 2024, with fractional heating).

Typically, a snowfall would lead to the radiometer being completely covered in snow, even with continuous heating. Since the hot air blown by the heating module could only exit around the radiometer lenses (see Fig. 10), the overlying snow melted quickly. However, once the melt opened an outlet for the hot air, it could exit the radiometer casing without melting any more snow.

https://doi.org/10.5194/egusphere-2026-2196
Preprint. Discussion started: 28 July 2026

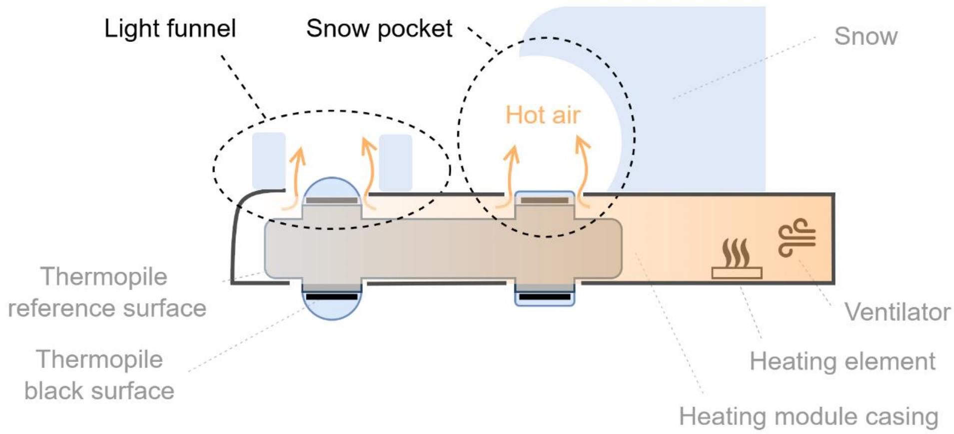

Fig. 10. Schematic view (cross section) of a net radiometer (CNR4) with a heater/ventilator installed; the orange background represents heat being pushed into the casing, slowly dissipating as it goes further up the radiometer.

4.3 Longwave measurements

The increased longwave signal from the snow-covered radiometer (section 3.5) occurred because the snow pocket surrounding the lens was warmer than the surrounding atmosphere (Lapo *et al.*, 2015; van den Broeke *et al.*, 2004). During such events, the control radiometer longwave signal was dominated by emissions from the nearby snow surface instead of the colder atmosphere.

Longwave radiation measurements are sensitive to the temperature of the sensor. Because substantial snow accumulation could have modified the heating efficiency, it was hypothesized that the sensor temperatures of the two devices may have differed. However, a comparison of the radiometer sensor temperatures over the full winter period showed an average difference of only 0.1 °C. Therefore, sensor temperature differences alone cannot explain the observed discrepancies in longwave radiation measurements.

https://doi.org/10.5194/egusphere-2026-2196
Preprint. Discussion started: 28 July 2026

The dominance of the longwave bias (+37.20 MJ m^{-2}) over the shortwave bias (−1.79 MJ m^{-2}) can be attributed to two factors : (1) incident solar radiation is modest in a forest gap in winter, particularly due to the low angles of incidence of the radiation, making the longwave contribution proportionally more significant, and (2) the longwave bias persists both day and night, whereas the shortwave bias is restricted to daylight hours (Malle *et al.*, 2019).

4.4 Shortwave measurements

When the radiometer was snow-covered, such as during periods following snowfall, the incoming shortwave radiation signal was attenuated because the snow obstructed the lens, resulting in reduced $SW_{\downarrow}$ values. This was more frequently observed when fractional heating was in place, as the heat from the CNF4 was not sufficient to remove snow for what could be many days. The diminished $SW_{\downarrow}$ signal – due to snow – is something that was also observed in other works on snowy radiometers (Cox *et al.*, 2021; Lapo *et al.*, 2015; van den Broeke *et al.*, 2004).

On clear-sky days, on the other hand, the signal could be underestimated or overestimated. An obstructed lens results in a reduced signal, while the light funnel effect results in an amplified signal, as shown in Fig. 8. As with the snow pockets on the pyrgeometer, hot air is blown out of the pyranometer lens, melting the snow as it passes. This creates a small, snow-free outlet for warm air to escape. The surrounding snow around the lens then reflects more light into the sensor, increasing the measured signal. Although this had been suggested by other studies (Lapo *et al.*, 2015), our results confirm the existence of this phenomenon through direct observation. However, as shown in Fig. 7c, the cumulative

https://doi.org/10.5194/egusphere-2026-2196
Preprint. Discussion started: 28 July 2026

effect of these measurement errors was less significant than that of the downwelling longwave measurements over the whole season. During continuous heating, on sunny days, a light funnel rapidly formed after a snowfall. On cloudy days, the predominance of diffuse shortwave radiation reduces the significance of this effect.

4.5 Net radiation

When the errors on longwave and shortwave measurements are combined, the bias on net radiation was close to zero under snow-free conditions, but rose to +0.742 MJ m^{-2} day^{-1} when snow covered the control radiometer. Note that the net radiation measurements of both devices perfectly overlap during the summer (Fig. A2a), whereas a pronounced gap can be observed in winter (Fig. 7a), which can be attributed to the presence of snow.

4.6 Fractional heating limitations

When heating was set on, the thermopile and the reference temperatures were changed, but not at the same rate, which resulted in irregularities in the measurements.

When heating was activated, the sensor's thermal equilibrium was disturbed, and the 5-min heating period was too short to stabilize the temperature across all thermopile components. During this transient phase, the reference surface warmed faster than the blackbody, reducing the temperature gradient and thus lowering the signal. This effect appears in all measurements and can be clearly seen in Fig. 4a–c: each time heating starts, the radiometer temperature rises and all measured signals decrease.

For longwave measurements, the signal is corrected using the sensor temperature (Fig. 4b). The upwelling longwave correction appears well synchronized with temperature, but for downwelling longwave, the validity of the correction is unclear. In all cases, partial or

https://doi.org/10.5194/egusphere-2026-2196
Preprint. Discussion started: 28 July 2026

intermittent heating introduces inconsistencies that fall beyond the scope of this study and should be avoided in radiometric measurements.

5 Conclusions

This study aims to measure the performance of a low-power snow removal device for radiometers, with the goal of improving the quality of radiation balance measurements. The proposed telescopic brush achieves this goal with minimal hindrance, using just 0.3% of the energy required by the traditional heating module, the latter being ineffective at removing snow. More specifically, this study compared measurements taken by a four-component radiometer equipped with both a heating module and an SRD with measurements taken by a radiometer equipped only with a heating module during the winter of 2024-25 in a forest gap of eastern Canada. Visual assessment revealed that the radiometer equipped with the SRD remained free of snow for most of the winter, except during periods when the SRD experienced freezing rain-induced failure. In such cases, the radiometer data had to be discarded.

Part of the study also examines the impact of continuous vs. fractional heating on the quality of incident radiation measurements. Results showed that using a ventilation-heating unit alone with a fractional heating schedule led to snow-covered device for several days after each snowfall. Fractional heating also resulted in a reduction of the longwave signal because of transient thermal states in the thermopile. We recommend heating for longer periods of time and less frequently.

On the other hand, using only a heating module continuously proved insufficient to generate robust results, as the flow of hot air creates air pockets in the snow accumulated around the lenses. For downwelling longwave radiation, the presence of snow on the device

https://doi.org/10.5194/egusphere-2026-2196
Preprint. Discussion started: 28 July 2026

resulted in artificially high radiation measurements, since the temperature of the accumulated snow was higher than the effective temperature of the surrounding canopy and atmosphere. For downwelling shortwave measurements, sunny days tended to lead to amplified signal due to the light funnel effect, but cloudy days were less affected.

For forest gaps such as the one proposed in this study, the increase in longwave dominated in contrast with the reduction of the downwelling shortwave radiation, mainly because these environments are almost always dominated by longwave exchanges. Consequently, a heated-only radiometer installed in this type of environment will overestimate net radiation.

Future work should assess model sensitivity to snow accumulation on radiometers by using this dataset to evaluate how measurement biases influence model outputs. Another avenue of research is the development of snow-detection algorithms, leveraging data from both the control and snow-cleared radiometers to identify snow obstruction events. In parallel, a next-generation SRD should be developed, with new requirements such as the ability to clear snow from its own housing to further minimize solid-angle biases caused by accumulation.

https://doi.org/10.5194/egusphere-2026-2196
Preprint. Discussion started: 28 July 2026

6 Appendix A

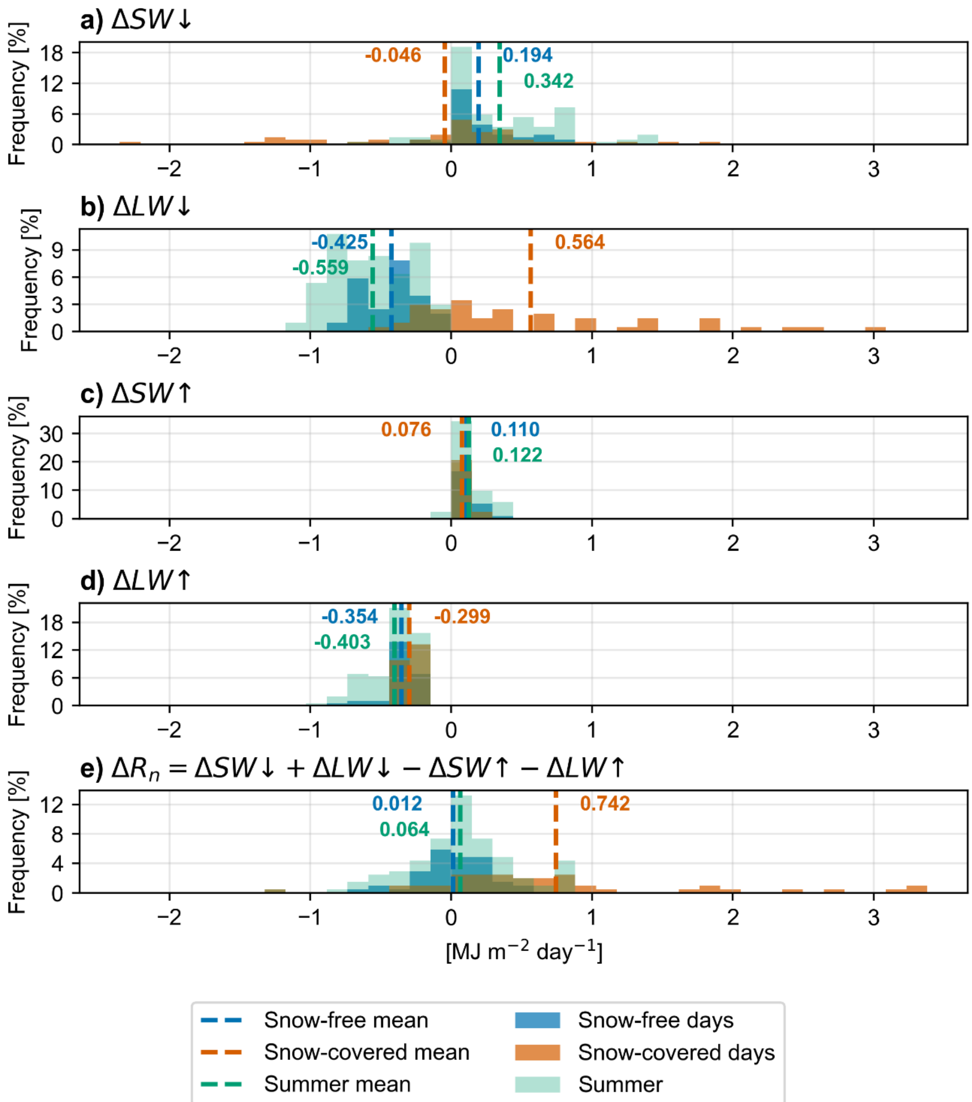

Fig. A1. Daily energy difference (control minus snow-cleared radiometer data) between the two radiometers represented as histograms and classified according to snow-free days (blue), snow-covered days (orange) and summer days (green). Dotted lines show the mean value (also printed out) of each group. Data are plotted from 1 January to 11 July 2025.

https://doi.org/10.5194/egusphere-2026-2196
Preprint. Discussion started: 28 July 2026

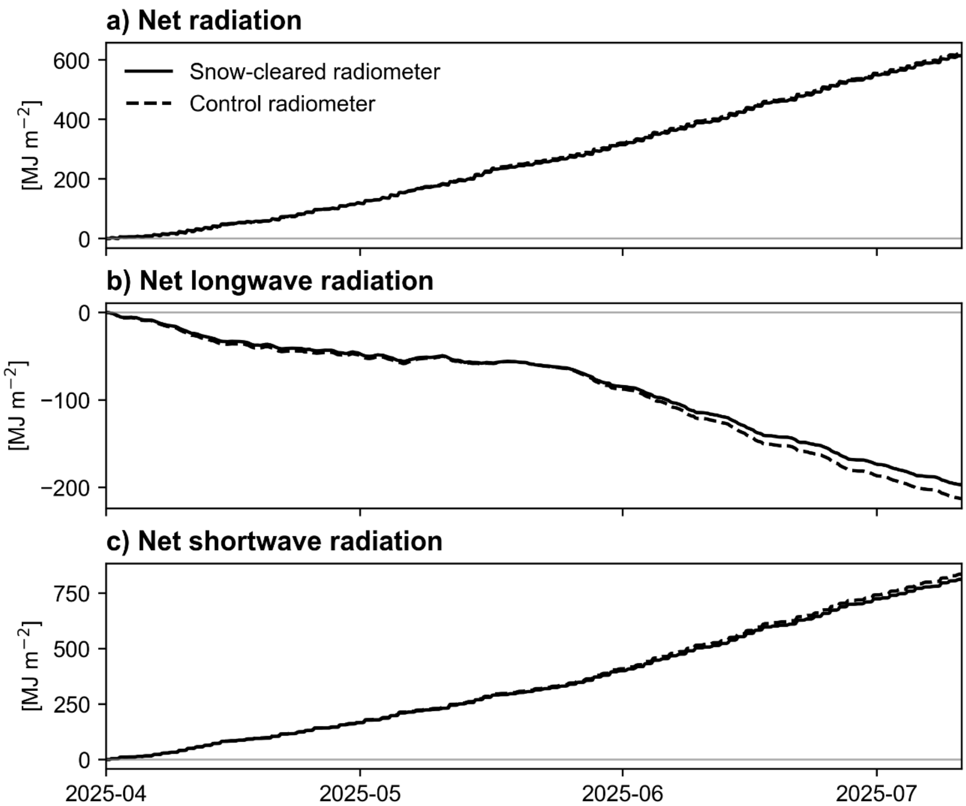

Fig. A2. Cumulative radiation from the two radiometers from 1 April 2025 to 11 July 2025: a) Net radiation; b) Net longwave radiation; c) Net shortwave radiation. The solid lines represent the snow-cleared radiometer, while the dashed lines represent the control radiometer.

7 Data availability

All research data presented in the article are original and were collected independently. The data have been published in the publicly accessible Borealis Canadian Dataverse Repository under the title *Data for "An automated snow-removal device for radiometers"* (https://doi.org/10.5683/SP3/DIO9JK).

8 Author contribution

JL carried out the experiment as part of his graduate studies. This included designing and assembling all the mechanical and electrical components for the setup at the NEIGE site. NB developed, manufactured and assembled the SRD. JL was responsible for data collection and interpretation. DFN and ABD acted as project managers, providing funding and managing resources, as well as guiding the data analysis and writing of the paper. BB and PEI reviewed the multiple versions of the paper.

9 Competing interests

The authors declare that they have no conflict of interest.

10 Acknowledgements

The authors would like to thank Sylvain Jutras and Vincent Grégoire for their valuable collaboration with data and logistics at the NEIGE site. We would also like to thank all the members of the HydroNord research group who helped with fieldwork: Dmitry Pershin, Katrine Trottier, Emmanuelle Barrette, Thomas Brady and Étienne Tremblay.
During the preparation of this work, the authors used ChatGPT and DeepL to rephrase sentences. After using this tool/service, the authors reviewed and edited the content as necessary, taking full responsibility for the content of the article.

11 Financial support

The authors would like to acknowledge the funding obtained from the Natural Sciences and Engineering Research Council of Canada through the Discovery Grant RGPIN-2023-

03484 (D.F. Nadeau) entitled "Water availability controlled by snow-forest interactions in cold and humid climates".

12 References

Aoki, T., Kuchiki, K., Niwano, M., Kodama, Y., Hosaka, M., & Tanaka, T. (2011). Physically based snow albedo model for calculating broadband albedos and the solar heating profile in snowpack for general circulation models. *Journal of Geophysical Research*, *116*(D11), D11114. https://doi.org/10.1029/2010JD015507

Beaudoin-Galaise, M., & Jutras, S. (2022). Comparison of manual snow water equivalent (SWE) measurements : Seeking the reference for a true SWE value in a boreal biome. *The Cryosphere*, *16*(8), 3199-3214. https://doi.org/10.5194/tc-16-3199-2022

Campbell Scientific. (2025). *Product Manual CNR4*. Campbell Scientific.

Cox, C. J., Morris, S. M., Uttal, T., Burgener, R., Hall, E., Kutchenreiter, M., McComiskey, A., Long, C. N., Thomas, B. D., & Wendell, J. (2021). The De-Icing Comparison Experiment (D-ICE) : A study of broadband radiometric measurements under icing conditions in the Arctic. *Atmospheric Measurement Techniques*, *14*(2). https://doi.org/10.5194/amt-14-1205-2021

Domine, F., Lackner, G., Sarrazin, D., Poirier, M., & Belke-Brea, M. (2021). Meteorological, snow and soil data (2013–2019) from a herb tundra permafrost site at Bylot Island, Canadian high Arctic, for driving and testing snow and land surface models. *Earth System Science Data*, *13*(9), 4331-4348. https://doi.org/10.5194/essd-13-4331-2021

https://doi.org/10.5194/egusphere-2026-2196
Preprint. Discussion started: 28 July 2026

Domine, F., Sarrazin, D., Nadeau, D. F., Lackner, G., & Belke-Brea, M. (2024). Meteorological, snow and soil data, CO_2 , water and energy fluxes from a low-Arctic valley of Northern Quebec. *Earth System Science Data*, *16*(3), 1523-1541. https://doi.org/10.5194/essd-16-1523-2024

Driemel, A., Augustine, J., Behrens, K., Colle, S., Cox, C., Cuevas-Agulló, E., Denn, F. M., Duprat, T., Fukuda, M., Grobe, H., Haeffelin, M., Hodges, G., Hyett, N., Ijima, O., Kallis, A., Knap, W., Kustov, V., Long, C. N., Longenecker, D., … König-Langlo, G. (2018). Baseline Surface Radiation Network (BSRN) : Structure and data description (1992-2017). *Earth System Science Data*, *10*(3). https://doi.org/10.5194/essd-10-1491-2018

Gaillard, M., Vionnet, V., Lafaysse, M., Dumont, M., & Ginoux, P. (2025). Improving large-scale snow albedo modeling using a climatology of light-absorbing particle deposition. *The Cryosphere*, *19*(2), 769-792. https://doi.org/10.5194/tc-19-769-2025

Heiskanen, J., Brümmer, C., Buchmann, N., Calfapietra, C., Chen, H., Gielen, B., Gkritzalis, T., Hammer, S., Hartman, S., Herbst, M., Janssens, I. A., Jordan, A., Juurola, E., Karstens, U., Kasurinen, V., Kruijt, B., Lankreijer, H., Levin, I., Linderson, M.-L., … Kutsch, W. (2022). The integrated carbon observation system in Europe. *Bulletin of the American Meteorological Society*, *103*(3), E855-E872. https://doi.org/10.1175/BAMS-D-19-0364.1

Huang, H., & Huang, Y. (2023). Diagnosing the radiation biases in global climate models using radiative kernels. *Geophysical Research Letters*, *50*(13), e2023GL103723. https://doi.org/10.1029/2023GL103723

Il Jeong, D., & Sushama, L. (2018). Rain-on-snow events over North America based on two Canadian regional climate models. *Climate Dynamics*, *50*(1-2), 303-316. https://doi.org/10.1007/s00382-017-3609-x

Irambona, C., Music, B., Nadeau, D. F., Mahdi, T. F., & Strachan, I. B. (2018). Impacts of boreal hydroelectric reservoirs on seasonal climate and precipitation recycling as simulated by the CRCM5 : A case study of the La Grande River watershed, Canada. *Theoretical and Applied Climatology*, *131*(3-4), 1529-1544. https://doi.org/10.1007/s00704-016-2010-8

Isabelle, P.-E., Nadeau, D. F., Anctil, F., Rousseau, A. N., Jutras, S., & Music, B. (2020). Impacts of high precipitation on the energy and water budgets of a humid boreal forest. *Agricultural and Forest Meteorology*, *280*, 107813. https://doi.org/10.1016/j.agrformet.2019.107813

Isabelle, P.-E., Nadeau, D. F., Asselin, M.-H., Harvey, R., Musselman, K. N., Rousseau, A. N., & Anctil, F. (2018). Solar radiation transmittance of a boreal balsam fir canopy : Spatiotemporal variability and impacts on growing season hydrology. *Agricultural and Forest Meteorology*, *263*, 1-14. https://doi.org/10.1016/j.agrformet.2018.07.022

Jin, J., Gao, X., Yang, Z.-L., Bales, R. C., Sorooshian, S., Dickinson, R. E., Sun, S. F., & Wu, G. X. (1999). Comparative analyses of physically based snowmelt models for climate simulations. *Journal of Climate*, *12*(8), 2643-2657. https://doi.org/10.1175/1520-0442(1999)012%253C2643:CAOPBS%253E2.0.CO;2

https://doi.org/10.5194/egusphere-2026-2196
Preprint. Discussion started: 28 July 2026

Kim, T., Zhou, W., Tran, V. N., Zhang, L., Wang, J., Zhu, M., Sheshukov, A. Y., Zhang, T., Liu, D., Mazepa, V. S., Sokolov, A. A., Valdayskikh, V. V., & Ivanov, V. Y. (2025). Biases in radiative flux observations due to precipitation across the Arctic forest-tundra ecotone. *Agricultural and Forest Meteorology*, *374*, 110814. https://doi.org/10.1016/j.agrformet.2025.110814

Kipp & Zonen. (2025). *Net Radiometer CNR4 Instruction Manual*. Kipp & Zonen. www.kippzonen.com

Lapo, K. E., Hinkelman, L. M., Landry, C. C., Massmann, A. K., & Lundquist, J. D. (2015). A simple algorithm for identifying periods of snow accumulation on a radiometer. *Water Resources Research*, *51*(9). https://doi.org/10.1002/2015WR017590

Liang, S., Stroeve, J., & Box, J. E. (2005). Mapping daily snow/ice shortwave broadband albedo from Moderate Resolution Imaging Spectroradiometer (MODIS) : The improved direct retrieval algorithm and validation with Greenland in situ measurement. *Journal of Geophysical Research: Atmospheres*, *110*(D10), 2004JD005493. https://doi.org/10.1029/2004JD005493

Long, C. N., & Shi, Y. (2008). An automated quality assessment and control algorithm for surface radiation measurements. *The Open Atmospheric Science Journal*, *2*(1). https://doi.org/10.2174/1874282300802010023

Lundquist, J. D., Wayand, N. E., Massmann, A., Clark, M. P., Lott, F., & Cristea, N. C. (2015). Diagnosis of insidious data disasters. *Water Resources Research*, *51*(5). https://doi.org/10.1002/2014WR016585

Malek, E. (2008). The daily and annual effects of dew, frost, and snow on a non-ventilated net radiometer. *Atmospheric Research*, *89*(3). https://doi.org/10.1016/j.atmosres.2008.02.006

Malle, J., Rutter, N., Mazzotti, G., & Jonas, T. (2019). Shading by trees and fractional snow cover control the subcanopy radiation budget. *Journal of Geophysical Research: Atmospheres*, *124*(6). https://doi.org/10.1029/2018JD029908

Matsui, N., Long, C. N., Augustine, J., Halliwell, D., Uttal, T., Longenecker, D., Niebergall, O., Wendell, J., & Albee, R. (2012). Evaluation of Arctic broadband surface radiation measurements. *Atmospheric Measurement Techniques*, *5*(2). https://doi.org/10.5194/amt-5-429-2012

Musselman, K. N., Pomeroy, J. W., & Link, T. E. (2015). Variability in shortwave irradiance caused by forest gaps : Measurements, modelling, and implications for snow energetics. *Agricultural and Forest Meteorology*, *207*. https://doi.org/10.1016/j.agrformet.2015.03.014

Novick, K. A., Biederman, J. A., Desai, A. R., Litvak, M. E., Moore, D. J. P., Scott, R. L., & Torn, M. S. (2018). The AmeriFlux network : A coalition of the willing. *Agricultural and Forest Meteorology*, *249*, 444-456. https://doi.org/10.1016/j.agrformet.2017.10.009

Pierre, A., Jutras, S., Smith, C., Kochendorfer, J., Fortin, V., & Anctil, F. (2019). Evaluation of catch efficiency transfer functions for unshielded and single-Alter-shielded solid precipitation measurements. *Journal of Atmospheric and Oceanic Technology*, *36*(5), 865-881. https://doi.org/10.1175/JTECH-D-18-0112.1

https://doi.org/10.5194/egusphere-2026-2196
Preprint. Discussion started: 28 July 2026

van den Broeke, M., van As, D., Reijmer, C., & van de Wal, R. (2004). Assessing and improving the quality of unattended radiation observations in Antarctica. *Journal of Atmospheric and Oceanic Technology*, *21*(9). https://doi.org/10.1175/1520-0426(2004)021%253C1417:AAITQO%253E2.0.CO;2